Applied Surface Science 256 (2010) 6179–6185

Contents lists available at ScienceDirect

Applied Surface Science

journal homepage: www.elsevier.com/locate/apsusc

Characterization of mesoporous VO_x/MCM-41 composite materials obtained via post-synthesis impregnation

Saeed B. Bukallah[a,*], Ali Bumajdad[b], Kamal M.S. Khalil[c], Mohamed I. Zaki[d]

[a] Department of Chemistry, Faculty of Science, UAE University, P.O. Box 17551, Al-Ain, United Arab Emirates
[b] Chemistry Department, Faculty of Science, Kuwait University, P.O. Box: 5969, Safat 13060, Kuwait
[c] Department of Chemistry, Faculty of Science, Sohag University, Sohag 82524, Egypt
[d] Chemistry Department, Faculty of Science, Minia University, El-Minia 61519, Egypt

ARTICLE INFO

Article history:
Received 7 January 2010
Received in revised form 17 March 2010
Accepted 17 March 2010
Available online 4 April 2010

Keywords:
MCM-41
VO_x/MCM-41 composites
Mesoporous
X-ray diffractometry
X-ray photelectron spectroscopy

ABSTRACT

Spherical-particle MCM-41 was synthesized at room temperature, and, then, impregnated with aqueous solutions of NH_4VO_3 to produce variously loaded VO_x/MCM-41 composite materials. Bulk and surface properties of the materials thus produced were characterized by means of X-ray powder diffractometry (XRD), infrared spectroscopy (FTIR), N_2 sorptiometry and X-ray photoelectron spectroscopy (XPS). Results obtained indicated that subsequent calcination at 550 °C (for 2 h) of the blank and impregnated MCM-41 particles, results in materials assuming the same bulk structure of MCM-41, and exposing uniformly mesporous, high area surfaces (P_w = 2.0–2.3 nm; 974–829 m^2/g), except for the material obtained at 20 wt%-V_2O_5 that was shown to suffer a considerable loss on surface area (down to 503 m^2/g). XPS results implied that the immobilization of the VO_x species occurs via interaction with surface OH/H_2O groups of MCM-41, leading to the formation of vanadate (VO_3^-) surface species, as well as minor V–O–Si and V_2O_5-like species. However, in all cases, the vanadium sites remained pentavalent and exposed on the surface.

1. Introduction

MCM-41, which stands for Mobil Composition of Matter No. 41 [1], is a pure silica material that shows a highly ordered hexagonal array of unidirectional, hexagonally shaped mesopores with a very narrow pore size distribution [1–3]. It has attracted researchers from many disciplines since its discovery in 1992 [1]. This has been largely owing to a wide range of applications in various fields; including catalysis, sorption, separation, removal of environmental pollutants, and electronic and optical devices [4,5]. However, the enormous interest in MCM-4 is due, essentially, to a number of specific properties [2,3]: a well-defined crystallographic structure, a uniform size distribution (2–10 nm), a specific pore volume (up to 1.3 mL/g), a high specific surface area (up to 1500 m^2/g), and high thermal and chemical stabilities. Consequently, MCM-41 has been regarded by catalysis chemists and engineers as being a catalytic grade material [3] that should be sought for specific catalytic performances [2].

Nevertheless, pure MCM-41, i.e. a 100%-silica material, shows limited catalytic applications [2]. This has been ascribed [2] to its neutral framework structure and low surface reactivity. Therefore, potential research efforts have been exerted to devise means and ways of modification of MCM-41 with catalytically functional additives, by means of incorporation, grafting, or loading of various metal or metal oxide species [2].

Modification of MCM-41 with vanadium–oxygen (VO_x) species has been the focus of active research in the very recent years [6–8]. It is worth noting, however, that VO_x-modified MCM-41 was first prepared some fifteen years ago by Reddy et al. [9]. Based on early characterization studies [10,11], performed on the materials then obtained [9], it was concluded that: (i) vanadium centers in the as-synthesized and calcined forms of VO_x-modified MCM-41 assume the same coordination state, and do not establish direct chemical bonding with the silicate framework, and (ii) vanadium occurs simultaneously in framework and extra-framework type of species. Ever since, these conclusions have been a subject of continuous debate, and experimental evidences for the exact nature of the vanadium–oxygen species thus established have been sought [5].

Various preparation methods of pure and modified MCM-41 materials have been attempted [2]. Accordingly, VO_x species are generally introduced via two different ways: (i) during the synthesis of the parent gel of MCM-41 (this way is described as direct synthesis, and the product is denoted V–MCM-41) or (ii) by the impregnation (or grafting) of the as-synthesized MCM-41 particles (this way is described as post-synthesis, and the

* Corresponding author. Fax: +971 3 7134232.
E-mail address: Saeed.Bukallah@uaeu.ac.ae (S.B. Bukallah).

0169-4332/$ – see front matter © 2010 Elsevier B.V. All rights reserved.
doi:10.1016/j.apsusc.2010.03.137

product is designated V/MCM-41). V–MCM-41 is usually prepared by a hydrothermal method using vanadyl sulfate hydrate and cetyl (hexadecyl) trimethyl ammonium bromide (CTAB) [12–14], whereas V/MCM-41 is often obtained by the grafting of vanadyl acetyl acetonate on MCM-41 [14,15].

Within the above context, however, the following preparative events have received general consensus: (i) a fine control over the porosity and morphology of pure MCM-41 is achievable at room temperature when a tetra-*n*-alkoxysilane (such as tetraethoxysilane, TEOS) is added to an aqueous solution of a cationic surfactant in the presence of ammonia as a catalyst and ethanol as a homogenizer [3,16] and (ii) a modified MCM-41 of a large exposure of the modifying species and high hydrophobicity is obtainable when the pure material is first prepared via the above described non-hydrothermal method, and the modifying species are introduced via post-synthesis techniques (impregnation or grafting) [17].

Therefore, the present investigation was carried out to prepare V/MCM-41 (at various vanadia loading levels) via impregnation of room-temperature-synthesized spherical MCM-41 particles. Subsequently, bulk and surface properties of the materials thus obtained were characterized by means of X-ray powder diffractometry (XRD), infrared spectroscopy (FTIR), N_2 sorptiometry and X-ray photoelectron spectroscopy (XPS). The principle objective of the present work was to help bridging existing gaps [2,5] in the current understanding of the nature of the vanadium–oxygen species thus established.

2. Experimental

2.1. Preparation

2.1.1. Chemicals

Cetyl trimethyl ammonium bromide (CTAB), a 98% pure C16TMABr product of Aldrich; tetraethoxysilane (TEOS), a 98% pure $Si(OC_2H_5)_4$ product of Sigma–Aldrich; ammonium vanadate, a AR-grade NH_4VO_3 product of Aldrich; oxalic acid, a AR-grade $H_2C_2O_4$ product of Aldrich; ammonia solution (25% NH_3), a Merck product; and an absolute ethyl alcohol, a C_2H_5OH product of Alfa Acer, were procured and used as received. All preparations were carried out at $22 \pm 1\,^{\circ}C$.

2.1.2. Procedure

Blank MCM-41 was prepared by a surfactant (CTAB) assisted sol–gel method, using TEOS as the source of silica and the method detailed elsewhere [3,16]. The resulting silica gel was filtered, washed, and dried at 90 °C for 24 h, and, then calcined at 550 °C for 3 h. The targeted calcination temperature was approached by heating at 1 °C/min.

V/MCM-41 materials containing 5, 10 and 20%-V_2O_3 (w/w) were prepared by incipient-wetness impregnation of MCM-41 particles with the appropriate aqueous solution of NH_4VO_3 and oxalic acid (1:2 molar ratio). The resulting materials were dried at 90 °C for 24 h, and, then calcined at 550 °C for 3 h by a heating rate of 1 °C/min.

For clarity, the VO_x-modified materials thus obtained are denoted below as V5, V10 and V20, where the Arabic numeral stands for the weight percentage of the modifier included. Hence, the blank MCM-41 is denoted V0, i.e. VO_x-free.

2.2. Characterization methods

2.2.1. X-ray powder diffractometry (XRD)

XRD patterns were obtained (at room temperature and $2\theta = 10–80^{\circ}$) using a Philips 1840 diffractometer (Netherlands), equipped with Ni-filtered Cu-K_α radiation ($\lambda = 0.15418$ nm). The measured patterns were matched with standard data [18] for crystalline phase identification purposes.

2.2.2. Fourier-transform infrared spectroscopy (FTIR)

FTIR spectra (averaged 40 scans at 4000–400 cm^{-1} and the resolution of 4 cm^{-1}) were taken from KBr-supported test samples, using a Nicolet FTIR Magna-IR 560 system (USA).

2.2.3. Scanning electron microscopy (SEM)

SEM micrographs were obtained, using a JEOL microscope model JSM-5600 (Japan). Test samples were coated with gold before examination.

2.2.4. Nitrogen sorptiometry

Nitrogen adsorption–desorption isotherms were measured (at −196 °C) according to the recommendations of the IUPAC [19], using a model 100 Autosorb, Quantachrome Instrument Corporation (USA). Prior to exposure to the adsorptive gas atmosphere, test samples were degassed to 0.1 Pa at 250 °C for 2 h. Specific surface area ($S_{BET}/m^2 g^{-1}$) and adsorption constant, c, were calculated using the BET equation [20]. Total pore volume ($V_p/cm^3\,g^{-1}$) was calculated at $p/p_0 = 0.95$. The pore width (P_w/nm) distribution over the range of (2–50 nm) was generated from the adsorption branch of the isotherms via BJH method [21]. Calculations were performed using Autosorb 1 software for windows (copyright, 1995–2003, Quantachrome Instruments).

2.2.5. X-ray photoelectron spectroscopy (XPS)

XPS spectra were recorded using a VG SCIENTIFIC 200 spectrometer (UK) using AlK_α radiation of 1486.6 eV, operating at 13 kV and 23 mA. The spectra acquisition and handling were carried out by means of an on-line ECLIPSE data system (UK). The test samples were compacted onto the sample holder (8 mm in diameter) in an ambient atmosphere, mounted and stored in the introduction chamber until a vacuum of 10^{-9} to 10^{-10} Torr (1 Torr = 133.4 Pa) was reached. Then, the sample was transferred to the analysis chamber for data acquisition (0.2 eV step; 250 ms dwell time; 0.7 eV resolution; up to 10 scan). The binding energy values (BE/eV) were determined with respect to the C(1s) line (284.6 eV) originating from adventitious carbon, and the standard deviation of the peak positions was estimated to be ±0.2 eV. The surface atomic percentage of the elements detected was calculated from the peak areas (in counts eV/s) with integral subtraction of the background. Composite photoelectron emission peaks were deconvoluted in order to resolve component peaks.

3. Results and discussion

3.1. XRD patterns

XRD patterns determined for pure and VO_x-modified MCM-41 are exhibited in the diffractograms stacked in Fig. 1. A diffractogram obtained for pure vanadia (V_2O_5) sample, which was prepared and calcined similarly at 550 °C, is also given in Fig. 1 for reference purposes. It is obvious from the figure that the diffractograms of the three modified materials (V5, V10 and V20) are quite similar to that of the pure MCM-41 (V0), in reflecting nothing but the amorphous-like nature of MCM-41 materials in the high-angle range scanned [22]. Thus, the loaded VO_x species did not manifest themselves in detectable, separate three-dimensional crystalline structures. Alternatively, the VO_x species are most likely dispersed in two-dimensional monolayer and/or non-crystalline structures in the three modified MCM-41 materials. On the other hand, the VO_x species did not cause detectable modifications to the initial structure of the host MCM-41 material.

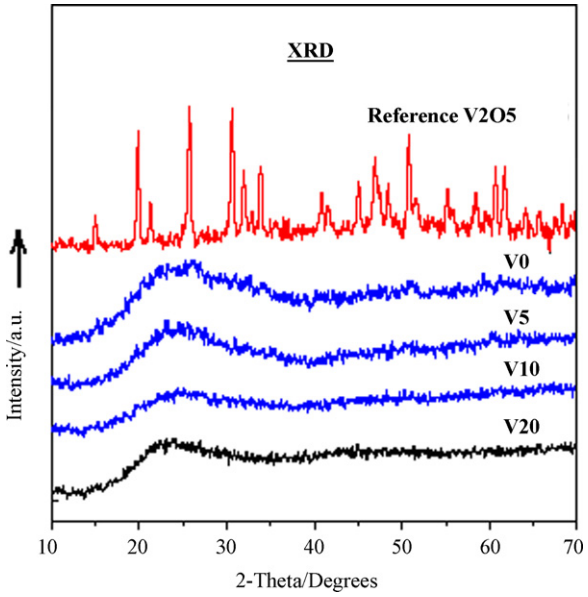

Fig. 1. X-ray powder diffractograms obtained for calcined, pure (V0) and VO_x-modified MCM-41 materials. The top diffractogram of bulk V_2O_5 is given for reference purposes.

3.2. IR spectra

Fig. 2 shows IR spectra recoded for the uncalcined (a) and calcined (b), pure and VO_x-modified MCM-41 materials. The spectra of the modified materials in each set (uncalcined or calcined) are shown to be closely related to that of the blank MCM-41 material (V0). Characteristic silica bands can be observed at 3430 cm^{-1} (νOH of associated silanol groups), 1630 cm^{-1} (δOH of water molecules), and ≤1440 cm^{-1}. The set of bands at ≤1440 cm^{-1} are

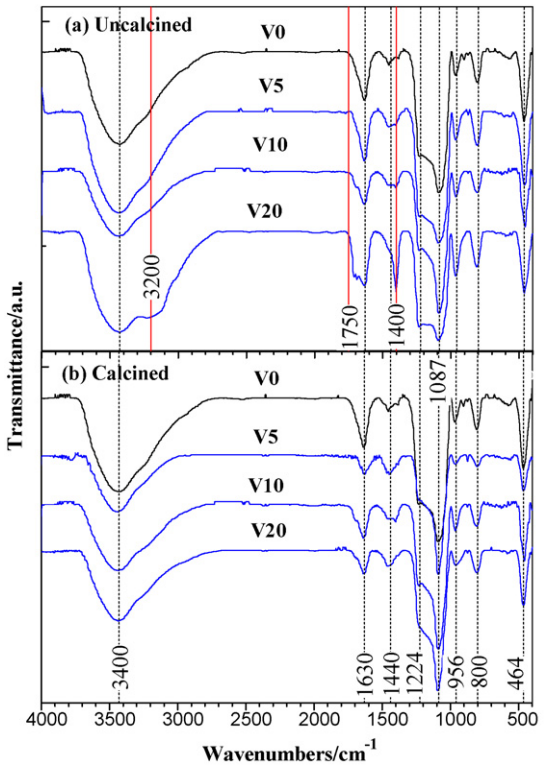

Fig. 2. FT-IR spectra taken of uncalcined (a) and calcined (b), pure and VO_x-modified MCM-41 materials.

due to silicon–oxygen framework vibration of MCM-41 [16,23]: the bands at 1224 and 1087 cm^{-1} are due to ν_{as}(Si–O–Si) vibrations; whereas, the bands at 956, 800 and 464 cm^{-1} are assignable respectively to ν_{as}(Si–OH), ν_s(Si–O–Si); and δ(Si–O–Si) vibrations. The absence of absorption near 3740 cm^{-1}, usually observed for silica-rich materials [23,24], may imply that isolated silanol (Si-OH) groups are either scarce or associated in hydrogen-bonding [24]. Moreover, three absorptions (at 3200, 1750 and 1400 cm^{-1}) are shown to grow stronger with the VO_x loading level of the uncalcined materials (Fig. 2(a)). These bands are indeed relevant to the impregnated NH_4VO_3 species, since they are assignable to stretching and bending vibrations of NH_4^+ ions [23]. A further support to this assignment is the fact that these bands are absent in the spectra of the corresponding calcination products (Fig. 2(b)), which may, on the other hand, be considered indicative of the complete decomposition of the impregnated NH_4VO_3 species upon calcination at 550 °C.

Accordingly, the IR spectra (Fig. 2) may help making two observations that are worth consideration. The first is to do with the absence of detectable absorptions (at 3000–2700 cm^{-1}) assignable to νCH vibrations reminiscent to surfactant species (CTAB). Whereas the second observation is to do with the modification conceded by the contour and intensity of the absorption at 956 cm^{-1} in the spectra of the calcination products (Fig. 2(b)), which is assignable to the rocking mode of vibration of Si–OH groups. Similar observations have been considered [17] to account for two different ways of introducing the thermally genesized VO_x species in the as prepared precursor (CTAM containing material): (i) by exchange with quaternary ammonium ions of the surfactant species, and/or (ii) by grafting of the vanadium precursor species via reaction of the latter with silanol groups. Lang et al. [17] have denied the former way, and have favored an alternative way, whereby the introduction of metal precursors is facilitated via interaction with Si–OH groups. Compatibly, modifications conceded by the concerned ν_{as}Si–OH absorption near 960 cm^{-1} have been attributed [25] to the incorporation of various heteroatoms into framework sites of porous metallo-silicates, which may correspond in the present case to framework Si–O–V stretching vibrations of V/MCM-41, and/or to perturbations in the silanol vibration due to adjacent VO_x ionic species [26]. Thus, for the present case, introduction of metal precursors in the calcined precursor (free from CTAB) is facilitated via interaction with Si–OH groups. Moreover, the absence of a peak near 820 cm^{-1} in the spectra obtained for the calcined materials (Fig. 2(b)), assignable to V–O–V deformation modes of crystalline V_2O_5 [27], confirms the absence of three-dimensional VO_x structures, which is in line with the XRD results (Fig. 1).

3.3. N_2 adsorption isotherms

Nitrogen adsorption–desorption isotherms determined (at −196 °C) on the different calcined materials are compared in Fig. 3. The isotherms are closely similar to the typical type-IV isotherm for MCM-41 materials [28]. They show an early gradual increase of the multilayer adsorption, followed by a relatively steeper increase at $0.20 < p/p_0 > 0.30$, which is indicative of capillary condensation inside narrow mesopores [3,28]. At higher relative pressures, the V5 and V10 materials show an extended plateau, thus implying the absence of pore filling (at $p/p_0 \geq 0.30$) in wider mesopores. In contrast, the isotherm determined on the V20 material displays a narrow hysteresis loop at $p/p_0 > 0.65$, thus revealing capillary condensation in wider mesopores.

Table 1 cites a typically high specific surface area of 907 m^2/g for V0 (the blank MCM-41) material. It shows, moreover, that the V5 and V10 materials assume comparably high specific surfaces areas (974 and 829 m^2/g, respectively), whereas the V20 material is shown to suffer a considerable loss on surface area (down

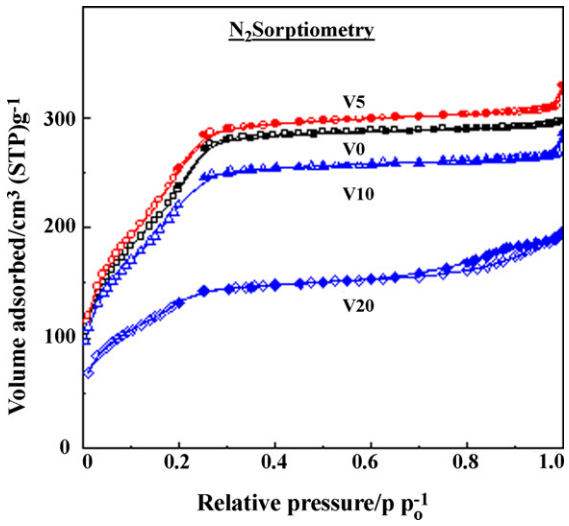

Fig. 3. N_2 adsorption–desorption isotherms determined (at −195 °C) on calcined, pure and VO_x-modified materials.

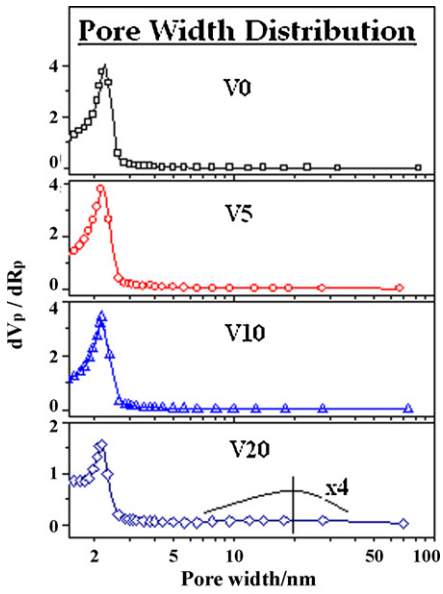

Fig. 4. BJH pore width distribution curves obtained for the calcined, pure and VO_x-modified materials.

to 503 m^2/g). A similar trend of variation is shown (Table 1) to be maintained by the total pore volume (V_p) value. On the other hand, the comparably low adsorption constant, c_{BET}, values (32–44) cited in Table 1 for the four test materials may imply that the modification with VO_x species did not alter significantly the surface chemistry of MCM-41. Furthermore, the modification with VO_x species is shown (Table 1) not to alter significantly the average pore width (P_w = 2.0–2.3 nm) of the blank V0-material (P_w = 2.0 nm). Hence, the results set out in Table 1 relate the sole detectable surface textural changes (the loss on surface area and pore volume) to increasing the loading level of VO_x to 20%. This relationship can be sustained by the pore width distribution curves (Fig. 4), which are similar in monitoring a single peak at P_w = 2.2 nm for the blank and the three modified materials, but show and additional broad peak, centered around P_w = 20 nm, only for the V20 material. This latter result may justify the display in the isotherm of V20 only of a high-relative-pressure hysteresis loop (Fig. 3).

3.4. Scanning electron micrographs

SEM micrographs were obtained for the calcination products of pure and VO_x-modified MCM-41 materials, but Fig. 5 only compares those obtained for the blank V0 (a) and the modified V20 material (b). The micrographs visualize the typical spherical morphology of the MCM-41 particles (400 ± 100 nm in diameter) [3]. The particles of V0, V5 and V10 were found to be non-agglomerated; i.e., loose. However, some appreciable particle aggregation can be observed for V20 in Fig. 5(b), which is most likely a consequence of the high-level VO_x-loading of the material. This result may presume that it was the surface structure assumed at such a high level of VO_x-loading that facilitated the observed particle aggregation on the indicated scale of magnification (Fig. 5(b)).

Table 1
Values of the BET surface area (S_{BET}) and *c*-constant (c_{BET}), and total pore volume (V_p) and pore width (P_w) as derived for calcined, pure and VO_x-modified MCM-41 materials.

Material	SBET/m^2 g^{-1}	c_{BET}	V_p/cm^3 g^{-1}	P_w/nm	
				Average	BJH
V0	907	32	0.456	2.0	2.2
V5	974	30	0.478	2.0	2.2
V10	829	37	0.412	2.0	2.2
V20	503	44	0.292	2.3	2.2

3.5. X-ray photoelectron spectra

The calcination products of pure and VO_x-modified MCM-41 materials were subjected to XPS surface analysis, in order to reveal the nature and oxidation state of the modifying VO_x species. The

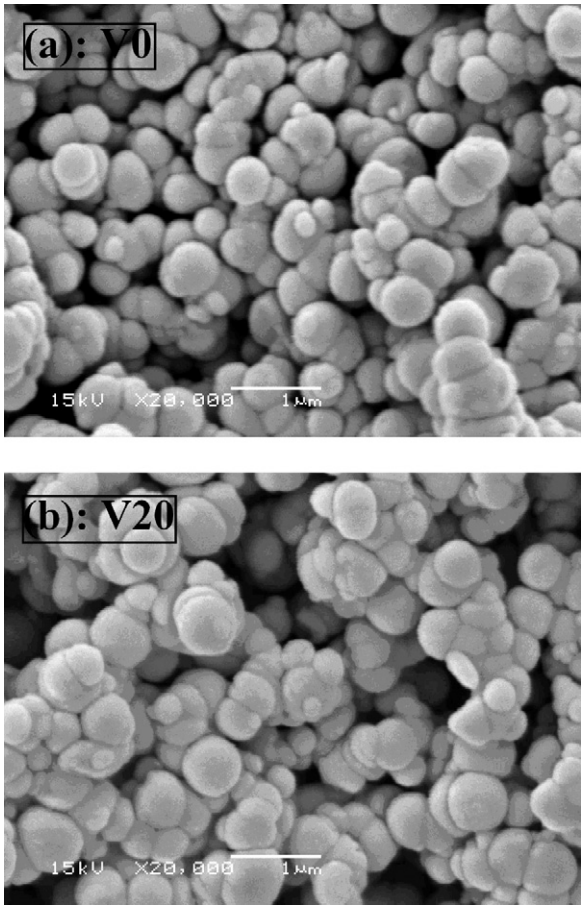

Fig. 5. SEM micrographs obtained for the calcined, pure (a) and 20 wt%-V_2O_5 modified (b) MCM-41.

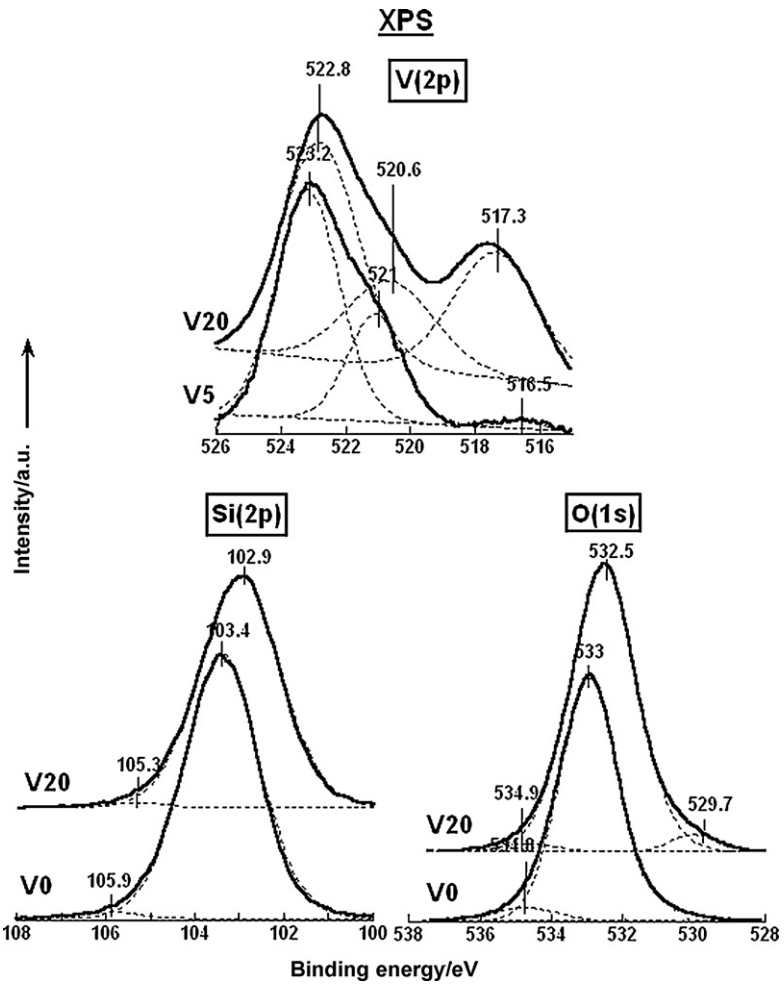

Fig. 6. Deconvoluted Si2p, O1s and V2p XPS spectra obtained for the indicated calcined, pure and modified MCM-41 materials.

analysis disclosed the exposure of carbon, oxygen and silicon atoms on all of the four test materials, in addition to vanadium atoms but only on surfaces of the modified materials (V5, V10 and V20). Si2p, O1s and V2p photoelectron emission spectra are compared for V0, V5 and V20 in Fig. 6. It is obvious from Fig. 6 that most of the peaks monitored are composite and, therefore, peak deconvolution was carried out to resolve the component peaks. Binding energy, assignment and atomic proportion corresponding to each of the peaks resolved are summarized in Table 2.

Table 2 indicates that the carbon detected is due to minor surface species (3.5–5%), which may be related to remains of the surfactant used and its oxidation products. The oxygen detected is due, mostly, to oxide (O^{2-}) ions of vanadium–oxygen (I) and silicon–oxygen (II) species, as well as oxygen of OH/H_2O species (III). The vanadium encountered belongs to three different types of V–O species: vanadate (VO_3^-) species (I), V–O–Si species (II), and V_2O_5-like species (III). On the other hand, the silicon is suggested to be related to SiO_2-like structure, where the resolved, weak peak near 105 eV is a satellite of the principle peak at ca. 103 eV.

Based on the total atomic proportions of oxygen, silicon and vanadium, as cited in Table 2, the O/Si atomic ratios that can be calculated for the modified materials (1.91–1.94) are very close to that (1.94) obtained for the pure MCM-41 material. The fact that these O/Si relative ratios are very close to that (2.0) expected for SiO_2 may imply that the added VO_x species did not alter significantly the SiO_x stoichiometry of the host's surface. On the other hand, the V/Si relative proportion that can be calculated from the total atomic proportions of the two elements (Table 2) would be found to increase (from V/Si = 0.13 up to 0.18) with the VO_x-loading level (from 5 up to 20 wt%). This result may imply spreading of VO_x species on the host's surface.

Considering the relative atomic proportions of the three oxygen species resolved (I–III; Table 2), calculated ratio for oxygen species I/II is found to increase (from 0.018 up to 0.039) with the VO_x-loading level, whereas that calculated for oxygen species III/II is found to decrease (from 0.043 down to 0.023). These results may consolidate the suggestion put-forward in the literature [3] favoring the introduction of VO_x species via interaction with OH/H_2O atomic groups of MCM-41. On the other hand, the trend of variation of the atomic proportion determined for the three different species resolved for vanadium, as a function of the VO_x-loading level, may help suggesting that the initial vanadate (VO_3) precursor species remain as the major VO_x-species (3.3–3.1%), whereas the minor $VSiO_x$ species increase with the loading level (from 0.7 up to 1.1%). On the other hand, the third type of vanadium–oxygen species, i.e. the V_2O_5-like species, emerge on the V10 material and increase (from 0.6 up to 1.1%) on the V20 material.

The above XPS analysis results may imply that the introduction of the VO_x species occurs most likely via interaction with surface OH/H_2O groups of MCM-41, leading largely to the anchorage of the precursor vanadate (VO_3^-) species. Moreover, minor V–O–Si and V_2O_5-like species are also established on the surface, with the latter species being formed at $\geq$10 wt%-VO_x. In all cases, however, the vanadium sites remain pentavalent and exposed on the surface.

Table 2
Binding energy (BE), assignment[a], and atomic proportion (%)[b] for peaks resolved by deconvolution of XPS spectra obtained over the C1s, O1s, V2p and Si2$p_{3/2}$ photoelectron emission regions for surfaces of calcined, pure and VO_x-modified MCM-41 materials.

Material	Surface chemical composition and corresponding XPS characteristics											
	C1s			O1s			V2$p_{3/2}$			Si2$p_{3/2}$		
	(I) C–C/C–H	(II) C–O	(III) O=C–O/O=C–H	(I) O^{2-}/VO	(II) O^{2-}/SiO	(III) OH/H_2O	(I) $V^{5+}/(VO_y)^{x-}$	(II) V^{5+}/$VSiO_x$	(III) V^{5+}/V_2O_5	(I) Si^{4+}/SiO_2	(II) Si^{4+}/SiO_2
BE/±0.5 eV	284.6	286.0	288.3	530	533	535	517	521	523	103	105
V0	4.8*			62.8*			–			32.4*	
	3.0	1.7	0.1	–	59.0	3.8	–	–	–	31.9	0.5
V5	3.5*			60.7*			4.0*			31.8*	
	2.0	1.5	–	1.0	57.2	2.5	3.3	0.7	–	27.2	4.6
V10	3.4*			60.1*			4.7*			31.0*	
	2.2	1.2	–	1.8	56.7	1.6	3.2	0.9	0.6	29.3	2.3
V20	5.0*			58.9*			5.6*			30.5*	
	3.5	1.5	–	2.2	56.7	1.3	3.1	1.1	1.5	30.0	0.5

[a] Assignments are suggested in accordance with the following corresponding references. C1s (I), (II) and (III): Ref. [29]; O1s (I): Ref. [30], (II): Ref. [31], and (III): Ref. [32]; V2$p_{3/2}$ (I): Ref. [33], and (III): Ref. [34]; Si2$p_{3/2}$ (I): Ref. [35].
[b] Asterisk (*)-labeled magnitudes are the total atomic percentages of the elements encountered on each test material, whereas those given underneath are those determined for each corresponding species.

4. Conclusions

The above presented and discussed results may help drawing the following conclusions:

1. The room-temperature preparation method applied leads to the synthesis of spherical particles of MCM-41 like material exposing uniformly mesporous (P_w = 2.0–2.2 nm), high specific area (907 m^2/g) surfaces covered with associated silanol groups.
2. The post-synthesis impregnation of the MCM-41 particles thus obtained with aqueous solutions of NH_4VO_3, at increasing loading level up to 20 wt%-V_2O_5, results in the establishment of dispersed vanadate species on the host's surface.
3. The subsequent calcination at 550 °C of the vanadate-impregnated MCM-41 particles, gives rise to materials assuming the same bulk crystalline structure and uniformly mesporous, high area surfaces (P_w = 2.0–2.3 nm; 974–829 m^2/g), except for the material obtained at 20 wt%-V_2O_5 that was shown to suffer a considerable loss on surface area (down to 503 m^2/g).
4. Anchorage of the precursor vanadate species occurs most likely via interaction with the OH/H_2O surface atomic groups of the host MCM-41.
5. The initial vanadate species remain, despite calcination, the major vanadium–oxygen species established on surfaces of MCM-41 at all loading levels accomplished.
6. Minor vanadium–oxygen species are manifested in the form of V–O–Si and V_2O_5 like species, with the latter being formed only at ≥10 wt% loading levels.
7. In all cases, however, vanadium sites assume the pentavalent state.

Acknowledgments

We would like to acknowledge the grants (14-03-2-11/08 and 04-03-2-11/04, made for one of us (S.B.B.)) from the Research Affairs at the UAE University for financial support and analytical facilities at the CLU. Moreover, we appreciate the excellent technical assistance found at the analytical units of SAF (GS01/01) of Kuwait University.

References

[1] C.T. Kresge, M.E. Leonowicz, W.J. Roth, J.C. Vartuli, J.S. Beck, Nature 359 (1992) 710.
[2] A. Taguchi, F. Schüth, Micropor. Mesopor. Mater. 77 (2005) 1.
[3] M. Grün, K.K. Unger, A. Matsumoto, K. Tsutsumi, Micropor. Mesopor. Mater. 27 (1999) 207.
[4] T. Linssen, K. Cassiers, P. Cool, E.F. Vansant, Adv. Colloid Interface Sci. 103 (2003) 121.
[5] S. Shylesh, A.P. Singh, J. Catal. 228 (2004) 333.
[6] S.A. Karakoulia, K.S. Triantafyllidis, A.A. Lemonidou, Micropor. Mesopor. Mater. 110 (2008) 157.
[7] T. Tsoncheva, L. Ivanova, R. Dimitrova, J. Rosenholm, J. Colloid Interface Sci. 321 (2008) 342.
[8] S.A. Karakoulia, K.S. Triantafyllidis, G. Tsilomelekis, S. Boghosian, A.A. Lemonidou, Catal. Today 141 (2009) 245.
[9] K.M. Reddy, I. Moudrakovski, A. Sayari, J. Chem. Soc., Chem. Commun. (1994) 1059.
[10] S. Gontier, A. Tuel, Micropor. Mater. 5 (1995) 161.
[11] Z. Luan, J. Xu, H. He, J. Klinowski, L. Kevan, J. Phys. Chem. 100 (1996) 19595.
[12] G. Grubert, J. Rathousky, G. Schulz-Ekloff, M. Wark, A. Zukal, Micropor. Mesopor. Mater. 22 (1998) 225.
[13] C.W. Lee, W.O. Lee, S.E. Park, Catal. Today 61 (2000) 137.
[14] J. George, S. Shylesh, A.P. Singh, Appl. Catal. A 290 (2005) 148.
[15] E.V. Kondratenko, M. Cherian, M. Baerns, D. Su, R. Schlögl, X. Wan, I.E. Wachs, J. Catal. 234 (2005) 131.
[16] K.M.S. Khalil, J. Colloid Interface Sci. 307 (2007) 172.
[17] N. Lang, P. Delichere, A. Tuel, Micropor. Mesopor. Mater. 26 (2002) 203.
[18] JCPDS, International Centre for Diffraction Data, PCPDFWIN, JCPDS-ICDD, 1995.
[19] K.S.W. IUPAC, D.H. Sing, R.A.W. Everett, L. Haul, R.A. Moscou, J. Pierotti, T. Rouquerol, Siemieniewska, Pure Appl. Chem. 57 (1985) 603.
[20] B. Brunauer, P.H. Emmett, P.H.E. Teller, J. Am. Chem. Soc. 60 (1938) 309.
[21] E.P. Barrett, L.G. Joyner, P.H. Halenda, J. Am. Chem. Soc. 73 (1951) 373.

[22] W. Yao, Y. Chen, L. Min, H. Fang, Z. Yan, H. Wang, J. Wang, J. Mol. Catal. A 246 (2006) 162.
[23] I.A. Degen, Tables of Characteristic Group Frequencies for the Interpretation of Infrared and Raman Spectra, Acolyte Publ., Harrow, UK, 1997.
[24] M.I. Zaki, H. Knözinger, Mater. Chem. Phys. 17 (1987) 201.
[25] J.R. Sohn, Zeolites 6 (1986) 225.
[26] G.N. Vayssilov, Catal. Rev. (1997) 209.
[27] B.M. Reddy, I. Ganesh, B. Chowdary, Catal. Today 49 (1999) 115.
[28] F. Rouquerol, J. Rouquerol, K.S.W. Sing, Adsorption by Powders and Porous Solids, Academic Press, London, 1999, pp. 415–425.
[29] A. Bumajdad, M.I. Zaki, J. Eastoe, L. Pasupulety, Langmuir 20 (2004) 11223.
[30] F. Werfel, O. Brummer, Phys. Scripta 28 (1983) 92.
[31] F.P.J. Kerkhof, J.A. Moulijn, A. Heeres, J. Electron. Spectrosc. Relat. Phenom. 14 (1978) 453.
[32] P.D. Schulze, S.L. Schaffer, R.L. Hance, D.L. Utley, J. Vac. Sci. Technol. A 1 (1983) 97.
[33] S.F. Ho, S. Contrarini, J.W. Rabalais, J. Phys. Chem. 91 (1987) 4779.
[34] P. Mezentzeff, Y. Lifshitz, J.W. Rabalais, Nucl. Instrum. Methods Phys. Res. B 44 (1990) 296.
[35] J.A. Kovacich, P. Lichtman, J. Electron. Spectrosc. Relat. Phenom. 18 (1980) 341.